Journal of the Taiwan Institute of Chemical Engineers 165 (2024) 105811

Contents lists available at ScienceDirect

Journal of the Taiwan Institute of Chemical Engineers

journal homepage: www.journals.elsevier.com/journal-of-the-taiwan-institute-of-chemical-engineers

Catalytic co-pyrolysis of oil palm empty fruit bunches (EFB) and surgical face mask (SFM) wastes: Thermo-kinetic study, ANN model fitting, and synergistic effect

Melvin Xin Jie Wee [a], Bridgid Lai Fui Chin [a,b,c,*], Agus Saptoro [a,d], Jiuan Jing Chew [e], Jaka Sunarso [e], Suzana Yusup [f], Abhishek Sharma [g]

[a] Department of Chemical and Energy Engineering, Faculty of Engineering and Science, Curtin University Malaysia, CDT 250, 98009, Miri, Sarawak, Malaysia
[b] Energy and Environment Research Cluster, Faculty of Engineering and Science, Curtin University Malaysia, CDT 250, 98009, Miri, Sarawak, Malaysia
[c] Centre of New and Sustainable Energy Research and Ventures (CoNSERV), Curtin University Malaysia, CDT 250, 98009, Miri, Sarawak, Malaysia
[d] Curtin Malaysia Research Institute (CMRI), CDT 250, Miri, 98009, Sarawak, Malaysia
[e] Research Centre for Sustainable Technologies, Faculty of Engineering, Computing and Science, Swinburne University of Technology, Jalan Simpang Tiga, 93350 Kuching, Sarawak, Malaysia
[f] Generation Unit (Fuel Technology & Combustion), Tenaga Nasional Berhad (TNB) Research Sdn Bhd, No. 1, Kawasan Institusi Penyelidikan, Jln Ayer Hitam, 43000 Kajang, Selangor, Malaysia
[g] Department of Biotechnology and Chemical Engineering, Manipal University Jaipur, Jaipur 303007, Rajasthan, India

ARTICLE INFO

Keywords:
Catalytic Co-pyrolysis
DAEM
Thermogravimetric analysis
HZSM-5
Synergistic effect
Artificial Neural Network (ANN)

ABSTRACT

Background: Catalytic co-pyrolysis process is an emerging thermochemical pathway to convert multiple wastes, such as biomass and municipal solid wastes into value added fuels. The ecology would suffer from mishandling of these materials, leading to landfills and microplastic contamination. However, the co-pyrolysis of the surgical face mask (SFM) wastes with biomass remains a niche research area.
Methods: The co-pyrolysis performance, kinetics and thermodynamics of oil palm empty fruit bunches (EFB) and SFM mixture were evaluated via thermogravimetric analysis (TGA) approach at heating rates from 10 to 100 °C. min^{-1} with weight ratio of 1:1, 4:1 and 1:4. Additionally, the development of the artificial neural network (ANN) model to represent the thermal degradation behaviour of the overall catalytic co-pyrolysis process for EFB and SFM mixtures.
Significant findings: The highest average pyrolysis performance index, I_r value of 8.11 was found in the reaction at 50 °C.min^{-1}. The weight change, ΔW_{TGA} showed the thermal degradation behaviour of EFB and SFM co-pyrolysis exhibited predominantly inhibitory characteristics, as the experimental values were higher than the theoretical values. Moreover, the HZSM-5 catalyst showed great affinity towards the sample matrix, achieving high reduction of activation energy and difference in enthalpy of 13.54 % and 14.94 %, respectively.

1. Introduction

The growing demand of the palm oil has made the oil palm sector a significant economical aspect for developing countries especially the top palm oil producers such as Indonesia, and Malaysia [1]. However, only 10 % of palm oil is being extracted from the total harvest [2]. The by-products, i.e., palm kernel shell, oil palm fronds, pressed fibres and empty fruit bunches (EFB) generate an abundant supply of solid wastes [3]. These biomasses are used as boiler fuel to produce steam and generate energy to the palm oil mill process [2-5]. While all carbonaceous feedstock produces carbon dioxide during thermal conversion, the direct combustion of biomass results in the immediate release of greenhouse gases (GHGs) into the atmosphere [1,6]. The alternative, pyrolysis, is able to recover and utilise the carbon species from the biomass in the products, i.e. syngas, bio-oil, and bio-char. These products can be utilised as a renewable energy source, contributing to the sustainability of the process [7]. Pyrolysis is an endothermic, inert, thermal conversion pathway, that can be applied to a wide variety of feedstock. It can be classified into slow, fast, and flash pyrolysis, which offers excellent control on the feedstock material and the desired

* Corresponding author.
E-mail address: bridgidchin@curtin.edu.my (B.L.F. Chin).

https://doi.org/10.1016/j.jtice.2024.105811
Received 17 April 2024; Received in revised form 24 September 2024; Accepted 21 October 2024
Available online 30 October 2024

Table 1
Summary of co-pyrolysis of biomass and plastic waste research direction.

Ref.	Feedstock/ Article type	Findings/summary
[10]	Review	Features the concept of co-pyrolysis of biomass and COVID-19 driven plastic waste. Summarises the findings of reported co-pyrolysis mechanisms. Explores the synergistic and antagonistic relationships between binary feedstocks with TGA data.
[11]	Review	Discusses the effect of parameters i.e., effect of feedstock properties, mixing ratio, temperature, and catalyst.
[12]	Review	Reports literature findings on the effect of operating conditions i.e. effect of time, temperature, mixing ratio and pressure. Delves into the reaction mechanisms of co-pyrolysis of biomass and plastic wastes.
[13]	Review	Reviews the co-pyrolysis of different types of plastics with biomass, co-pyrolysis at microscale and at bench scale, co-pyrolysis with different types of catalysts, and co-pyrolysis products.
[14]	Review	Reviews the co-pyrolysis of agricultural waste with disposable medical face mask. Summarises the key advances in this co-pyrolysis process and the kinetic studies.
[15]	**Biomass:** Pinewood **Plastics**: black polycarbonate (BPC), polyethylene terephthalate (PETE), and polypropylene (PP)	The study applied DAEM to study the thermo-kinetics for the co-pyrolysis of several recycled plastic waste with pinewood. Highest degree of synergy was observed with BPC plastic content of 50 % in pinewood, at 75 % for PETE in pinewood, and at 25 % for PP in pinewood. This shows that different plastic types would have different degrees of synergies with biomass with at different mixing ratios.
[16]	**Biomass:** kidney beans stalk **Plastic:** high density polyethylene (HDPE)	The kinetics was determined with Coats-Redfern method and Doyle's method. Introduces the synergistic effect calculation (ΔW) using the difference in experimental and theoretical DTG data. An ANN model was developed utilising the mass loss data from TGA and showed excellent performance ($R^2 = 0.9999$) in the prediction of the thermochemical behaviour of the feedstock samples.
[17]	**Biomass:** Corn stover, *narra*, and *ipil* **Plastic:** PP, low-density polyethylene (LDPE), and HDPE	Synergistic analysis quantified with the difference of mass loss rate from the TGA with theoretical values.
[25]	**Biomass:** Sawdust Plastic: Polystyrene (PS)	Co-pyrolysis of sawdust and polystyrene found highest synergy at 25 % PS content, which enhances the bio-oil yield from 31 % to 62 %.
[26]	**Plastic:** Mixed medical wastes	Pyrolysis of mixed medical wastes in a fixed bed reactor. The highest product distribution was at 500 °C with 57.1 % pyrolysis oil yield. Gas and char yield were 26.5–37.3 % and 24.2–12.4 %, respectively. Aromatics and cyclic hydrocarbons were the major compositions for the pyrolysis oil.
[28]	**Biomass:** Rapeseed stalk **Plastic:** Polyethylene terephthalate (PET), PP, and polyvinyl chloride (PVC)	Co-pyrolysis of biomass with plastics containing different elemental compositions, i.e. oxygen-rich PET, hydrogen-rich PP, and chlorine rich PVC. RS-PP co-pyrolysis obtained the highest hydrocarbon yield of 98.73 %. PP acts as a hydrogen donor for the cracking of aromatic structure of RS, which enhanced hydrocarbon conversion.

products [8,9].

Following this, recent biomass conversion studies employ the idea of co-pyrolysis as a pathway to reduce multiple wastes, such as biomass and municipal solid wastes. From the studies, co-pyrolysis has gained attraction, as an effective technique to convert these wastes to valuable fuels. Current studies of co-pyrolysis of biomass with plastic wastes in other studies include review articles [10-14], microscale thermo-kinetic studies [15-21], and the synthesis of biofuels using a pyrolyser set up [22-27] and their findings summarised in Table 1. The benefits for mixing biomass with plastic wastes include the high hydrogen and low oxygen content, which balance the features of the biomass which has high oxygen content [13]. The high oxygen content of the feedstock could result in low calorific and thermally unstable biofuel [24]. Furthermore, mixed wastes pyrolysis could also help to lower the activation energy, E of the pyrolysis process. According to Salvilla et al. [17], researchers reported the E of high-density polyethylene plastic (HDPE) reduced with the addition of *Ipil* and *Nara* biomass samples, 66 % and 24 %, respectively (at 1:1 feedstock ratio). Similar trend was also reported in the pyrolysis of kidney bean stalk with HDPE, where the reduction of E was 35 %. Following this, lowering the E would help in reducing the operational cost, thus improving the sustainability of the pyrolysis process.

Hence, it would be beneficial to apply this conversion technique to the plastic waste issue brought upon by the COVID-19 pandemic. These COVID-19 related wastes can be divided into two main categories namely waste generated from the medical institutions (i.e., medical bottle, N95 face masks and syringes), and waste generated from the public for social distancing purposes (i.e., surgical medical face masks (SFM), and rubber gloves) [29]. This research work aims to focus on the latter, as the waste management for these wastes are not under controlled as the medical wastes from the medical institutions. Mismanaging these wastes would be detrimental to the environment, causing microplastic pollution, and landfills [30,31]. Several studies from literatures began investigating the thermal degradation behaviours of SFM as a potential solution to manage these wastes [32-35]. In summary, the experiments showed promising pyrolysis characteristics of SFM wastes, which include high yield, high volatile matter content, and high selectivity to aromatic compounds. However, the co-pyrolysis of these SFM wastes with biomass remains a niche research area.

Furthermore, catalysts also play a role in enhancing the co-pyrolysis process and product upgrading, this process is known as the catalytic co-pyrolysis (CCP). Zeolite based catalyst such as HZSM-5 is one of the most common catalysts utilised in the CCP process. HZSM-5 has both the Lewis acid sites and Brønsted acid sites, which facilitates the dehydration, decarbonylation, decarboxylation, dehydrogenation, dealkylation, oligomerisation and Diels-Alder reaction, to remove oxygen content from the liquid fuels [24]. The CCP of biomass and plastic waste and its thermal degradation behavior is not well understood. Its performance could potentially minimize the energy requirement for co-pyrolysis, enhancing the sustainability of the process.

Besides that, artificial neural network (ANN) is gaining attention as a highly effective model prediction tool. It functions similarly to the human brain and neurons, i.e. able to process large amounts of data, and providing real time predictions. The utilisation of this tool to model fit the pyrolysis and co-pyrolysis process has been increasingly gaining attention due to its ability to adapt and predict to non-linear relationships [36]. Nawaz and Kumar [37] employed ANN to model fit the pyrolysis of SFM, obtaining a trained ANN model with the accuracy of R-squared, $R^2 = 0.99998$, and mean squared error (MSE) $= 2.7 \times 10^{-4}$. Similarly, Wang et al. [38] applied ANN for the model fitting of tobacco straw pyrolysis. The model trained achieved a $R^2 = 0.99999$ and mean squared error (MSE) $= 7.51 \times 10^{-3}$. Moreover, Mohan et al. [39] employed ANN for the co-pyrolysis of waste seed, and LDPE. The co-pyrolysis behaviour was perfectly adapted in the model with a R^2 and MSE of 1.00 and 2.21×10^{-11}, respectively. To the best of our knowledge, there is a lack of study on the prediction of the CCP of EFB and SFM

with HZSM-5 over the ANN model.

The determination of kinetic and thermodynamic parameters for the co-pyrolysis of biomass-plastic waste is imperative to designing an energy efficient and sustainable process. Thermogravimetric analysis (TGA) is a powerful tool to elucidate the kinetic mechanisms of thermochemical conversion of biomass and plastic wastes. The kinetic parameters were processed through model-free methods or isoconversional kinetic models i.e. Kissinger-Akihara-Sunose (KAS), and Flynn-Wall-Ozawa (FWO). These models assume solid-state samples follows a single-step volatilisation mechanism [40], and allows the determination of activation energy *via* a function of the extent of conversion with no prerequisite requirement of the decomposition reaction mechanism [41]. However, as the process becomes much complex with the addition of a secondary feedstock. Iso-conversional models becomes inadequate to explain the complex reaction kinetics. Therefore, the DAEM was chosen as the kinetic model in this study. The model assumed the co-pyrolysis process occurs through several parallel reactions [42]. It is a suitable model to represent the physical and heterogeneity of the co-pyrolysis process [43]. The multi-reaction model also can be well adapted in a broad range of heating rates and pyrolysis temperature [42]. Moreover, DAEM has been adapted to study the mechanisms of co-pyrolysis, and CCP processes [15,44,45].

Although there are various studies reported on the co-pyrolysis of biomass and plastic wastes, there are no data available to determine the co-pyrolysis reaction kinetics of EFB and SFM. Most of the co-pyrolysis of biomass with plastics in literature employs pure plastics as the feedstock. However, to address the underlying surge of plastic wastes, which are usually found as composites of different types of plastics, this paper had selected SFM (composed of polyolefin plastics i.e. PP and PE) as the co-feedstock for the co-pyrolysis reaction. Hence, this paper aims to determine the thermo-kinetic parameters for the catalytic co-pyrolysis of EFB and SFM and its mixtures through DAEM on the TGA data conducted. Thus, determining the configuration with the lowest *E*. Following this, to explore the synergistic interactions between EFB and SFM, and the influence of a catalyst (HZSM-5). The synergistic studies performed can reveal the significance of the interaction between EFB and SFM pyrolysis intermediates, which can imply reduction in the thermal requirements of the catalytic co-pyrolysis reaction system. Moreover, the development of the ANN model to represent the thermal degradation behaviour of the overall catalytic co-pyrolysis process for EFB and SFM.

2. Methods

2.1. Sample acquisition, preparation, and characterisation

The oil palm biomass, EFB was provided by Sarawak Oil Palms Berhad (SOPB) and was dried in a convection oven for 24 h with the temperature setting of 105 °C, to remove the moisture content. The dried EFB were grounded and sieved to <500 μm. The SFM were acquired from the brand *Pomerol*, the metal strip and cotton straps were removed. The filter layers of the SFM were cut and sieved to <500 μm. The feedstock samples were characterised *via* proximate analysis (TGA/DSC 3+, *Mettler Toledo,* ASTM D7582–12) and ultimate analysis (Vario MICRO, *Elementar*, ASTM D3176–09), to determine the macro-contents and elemental contents of the samples. The HZSM-5 catalyst was acquired from the manufacturing brand, *Alfa Aesar*. added *in-situ* with a 10 wt.% of the total weight of the EFB-SFM mixture (1:1, 1:4, 4:1). The selection of the weight ratios were studied by Ruiz-Montoya et al. [46] for biomass-HDPE co-pyrolysis, which showed significant *E* reduction compared to their mono-feedstock counterparts. Besides that, Anh Vo et al. [47] also utilised only 20 wt.% PP in the study of bamboo-polystyrene co-pyrolysis process to emphasise the role of biomass. Hence, to emphasise the role of EFB and SFM, the feedstock weight ratio of 1:4 and 4:1 for EFB:SFM was selected. Furthermore, the equal parts (1:1) feedstock weight ratio was employed in several studies on co-pyrolysis [39,48-52].

2.2. Thermogravimetric analyser (TGA) experiments

All the thermal degradation experiments were performed on the *Seiko EXSTAR TG/DTA 6300* thermogravimetric analyser (TGA) with heating rate settings of 10, 20, 50 or 100 °C.min^{-1}. The broad range of heating rates are selected to represent the heating conditions of the slow to fast pyrolysis process as conducted in these studies [53,54]. Firstly, purging of the TGA were performed by flowing the inert nitrogen gas (N_2, 5 N purity) at a constant flowrate of 100 mL.min^{-1} for 5 min at room temperature, to ensure an inert environment in the pyrolysis process. Next, the samples loaded onto a platinum crucible was heated non-isothermally from temperature 50 °C to 900 °C. The limitation of the study can arise from a few factors such as, heterogeneity of the sample (obvious in case of co-pyrolysis), instrument calibration, and vibrations in the platform. Hence, the first 20 % of the TGA, and data with linearity, $R^2 < 0.8$ are not considered in the computation of thermo-kinetic parameters.

2.3. Synergistic effect study between EFB-SFM mixture co-pyrolysis

For co-pyrolysis technique, it is important to investigate any synergistic effect between the biomass-plastic matrix. Hence, in the TGA blend ratio experiments, the difference in weight with respect to temperature (ΔW_{TGA}), and weight loss rate (ΔW_{DTG}) between the experimental and theoretical results are computed to evaluate if the EFB and SFM mixture exhibit inhibitory or synergistic relationship [17,55]. The equations below depict the theoretical values (denoted with *Th* subscript) from TGA Eq. (1) and DTG Eq. (2), and the differences of these values with respect to experimental (denoted with *Exp* subscript) TGA Eq. (3) and DTG Eq. (4) are represented as follows:

$$W_{TGA,Th} = x_{EFB} TGA_{EFB} + x_{SFM} TGA_{SFM} \quad (1)$$

$$W_{DTG,Th} = x_{EFB} DTG_{EFB} + x_{SFM} DTG_{SFM} \quad (2)$$

$$\Delta W_{TGA} = W_{TGA,Exp} - W_{TGA,Th} \quad (3)$$

$$\Delta W_{DTG} = W_{DTG,Exp} - W_{DTG,Th} \quad (4)$$

2.4. Pyrolysis performance index, I_r

The pyrolysis performance index is introduced by [56] as a method to evaluate the feedstock reactivity based on the expression as Eq. (5):

$$I_r = \frac{\left(\frac{d\alpha}{dt}\right)_{max} \cdot \alpha_{\Delta T}}{T_p \cdot T_i \cdot T_f} \quad (5)$$

where $\left(\frac{d\alpha}{dt}\right)_{max}$ is the maximum degradation rate, $\alpha_{\Delta T}$ is the degree of conversion of the degradation peak, T_p is the temperature at the peak (°C), T_i is the initiation temperature of the degradation peak (°C), and T_f is the offset temperature of the degradation peak (°C). The index relies on the feedstock conversion, feedstock energy content, pyrolysis time, and energy consumption. For an effective pyrolysis process, the goal is to maximize I_r by increasing feedstock conversion and reducing pyrolysis time. The numerator parameters, such as fractional feedstock conversion and heating value of feedstock, should be high, while pyrolysis time and energy consumption should be low. Utilising this index allows us to evaluate the suitability of feedstock for pyrolysis and enhance the process to decrease energy consumption [57].

2.5. Model fitting with artificial neural network (ANN)

An ANN model was trained in this work with heating rate and tem-

Table 2
ANN model construction configurations.

Constrains	Configurations
Network architecture	2 × 10 × 1
Input data	• Temperature • Heating rate
Output data	Weight %
Training algorithm	Levenberg-Marquardt
Data division method	dividerand

perature as the inputs, and weight loss (wt.%) as the output variable. The purpose of developing an ANN model is to predict and represent the thermal degradation behaviour catalytic co-pyrolysis process of EFB and SFM. The model was constructed in the *MATLAB R2022b* software with the neural network toolbox installed. The feedforward algorithm was selected as the supervised training algorithm. A total of 1730 dataset was divided randomly into training (70 %), testing (15 %), and validation (15 %), further details are summarised in Table 2 to develop the prediction model. The mean square error (MSE) in Eq. (6) was computed to evaluate its training progress at each epoch until the minimal MSE value has been achieved or the maximum epoch has reached. Besides that, the coefficient of determination (R^2) in Eq. (7) was further employed to evaluate the regression of the ANN model created.

$$MSE = \frac{1}{N}\sum_{i=1}^{N}\left(y_i - y_{i,\ model}\right)^2 \tag{6}$$

$$R^2 = 1 - \frac{\sum_{i=1}^{N}\left(y_i - y_{i,\ model}\right)^2}{\sum_{i=1}^{N}\left(y_i - \overline{y_i}\right)^2} \tag{7}$$

where N is the number of data, y_i is the target value, $y_{i,model}$ is the network output, and $\overline{y_i}$ is the mean of the target values. Besides that, the CCP of EFB and SFM mixture at 1:1 ratio and 30 °C min^{-1} heating rate were conducted. Its TGA results are compared with the prediction results from the trained ANN model to validate its accuracy in predicting a foreign parameter i.e., 30 °C.min^{-1} heating rate.

2.6. Kinetic model and parameters

The pyrolysis reaction is defined as the thermal degradation of a material with an absence of oxygen. To perform kinetic analysis, TGA data obtained can be processed via a suitable kinetic model. In this study, the multi-reaction model, DAEM is selected to compute the kinetic parameters for the co-pyrolysis of EFB and SFM. The DAEM assumes multiple first order reaction occurring simultaneously, each having its own E, and pre-exponential factor, A [42,58]. The generalised equation for DAEM can be described as Eq. (8) [45]. Where V, V^*, t, R, and T, are the volatiles mass fraction at any given time or temperature, the total volatile mass fraction, time (s), the universal gas constant (8.314 $J.mol^{-1}.K^{-1}$), and temperature (K) respectively. Furthermore, the V/V^* can be represented as the degree of conversion, α by following Eq. (9), where m_f represents residual weight of the feedstock sample, m_i is the initial weight of the feedstock sample, and m_t is the mass at any given time and temperature. In addition, the model assumes the E follows a distribution function, $f(E)$ [42]. Most studies employ the Gaussian distribution function as a solution for $f(E)$, which are given as Eq. (10) [59]. However, there are other existing methods that are available, i.e., Weibull [60], and logistic distribution [61].

$$1 - \frac{V}{V^*} = \int_0^{\infty} \exp\left(-A\int_0^{t}\exp\left(-\frac{E}{RT}\right)dt\right) f(E)dE \tag{8}$$

$$\frac{V}{V^*} = \alpha = \frac{m_f - m_t}{m_f - m_i} \tag{9}$$

$$f(E) = \frac{1}{\sigma\sqrt{2\pi}}\exp\left[-\frac{(E - E_o)^2}{2\sigma^2}\right] \tag{10}$$

where E_o, represents the initial guess activation energy and σ represents the standard deviation. While the inner integral dt can be represented as φ(t), and given that $T = T_0 + \beta t$, the integral can be rewritten in terms of temperature, T (K), or φ(E, T), as shown in Eq. (11).

$$\varphi(t) = \exp\left(-A\int_0^{t}\exp\left(-\frac{E}{RT}\right)dt\right) \cong exp\left(-\frac{A}{\beta}\int_0^{T}\exp\left(-\frac{E}{RT}\right)dT\right) \tag{11}$$

where the β represents the heating rates. Following this, Miura and Maki [62] introduced a simplified method of approximating the integral φ(E, T) Eq. (12), and substituting the correlation φ(E, T) = 1 − V/V^* = 0.58, forms Eq. (13).

$$\varphi(E,T) = exp\left(-\frac{A}{\beta}\int_0^{T}\exp\left(-\frac{E}{RT}\right)dT\right) \cong exp\left[\frac{ART^2}{\beta E}\exp\left(-\frac{E}{RT}\right)\right] \tag{12}$$

$$1 - \frac{V}{V^*} = exp\left[\frac{ART^2}{\beta E}\exp\left(-\frac{E}{RT}\right)\right] \tag{13}$$

Next, taking natural logarithm on both sides, and rearrange to form Eqs. (14) and (15). The value of 0.58 to the term (1 − V/V^*) and rearrange, forms a linear representation of the DAEM in Eq. (16).

$$\ln\left(1 - \frac{V}{V^*}\right) = \ln\left\{exp\left[\frac{ART^2}{\beta E}\exp\left(-\frac{E}{RT}\right)\right]\right\} \tag{14}$$

$$ln\left(\frac{\beta}{T^2}\right) = ln\left(\frac{AR}{E}\right) - ln\left[-ln\left(1 - \frac{V}{V^*}\right)\right] - \frac{E}{RT} \tag{15}$$

$$ln\left(\frac{\beta}{T^2}\right) = ln\left(\frac{AR}{E}\right) + 0.675 - \frac{E}{R}\cdot\frac{1}{T} \tag{16}$$

With the linear expression, Arrhenius plots for each sample and mixtures could be obtained by plotting the ln(β/T^2) to ($1/T$), with varying points of conversion. The E and A is obtained from the slope, ($-E/R$) and the intercept, $ln(AR/E)$ + 0.675 of the linear fitting line.

2.7. Thermodynamic parameters and analysis

The kinetic model selected for this project is the DAEM as shown in Eq. (8), and the procedure of the kinetic analysis was adopted but not limited to the study from Ng et al. [45], to compute the E and A values necessary for thermodynamic analysis. The thermodynamic parameters, change in enthalpy (ΔH), change in Gibbs free energy (ΔG), and change in entropy (ΔS) were computed via Eqs. (17)-(19), respectively.

$$\Delta H = E - R\cdot T \tag{17}$$

$$\Delta G = E + R\cdot T_m\cdot\ln\left(\frac{k_B\cdot T_m}{h\cdot A}\right) \tag{18}$$

$$\Delta S = \frac{\Delta H - \Delta G}{T_m} \tag{19}$$

where T_m, k_B and h refers to the mass loss temperature (K), Boltzman constant (1.38 × 10^{-23} $J.K^{-1}$), and the Planck's constant (6.626 × 10^{-34} $J.s$), respectively.

Table 3
Ultimate and proximate analysis of EFB and SFM.

Sample	EFB	SFM
Proximate analysis		
Moisture, wt.%	8.80	0.00
Ash, wt.%	3.22	0.23
Volatile matter, wt.%	72.08	97.21
Fixed carbon, wt.%	15.90	2.56
Ultimate analysis		
Carbon (C), wt.%	44.82	84.63
Hydrogen (H), wt.%	5.23	15.18
Oxygen (O), wt.%	49.88	0.00
Nitrogen (N), wt.%	0.07	0.00
Sulphur (S), wt.%	–	0.19

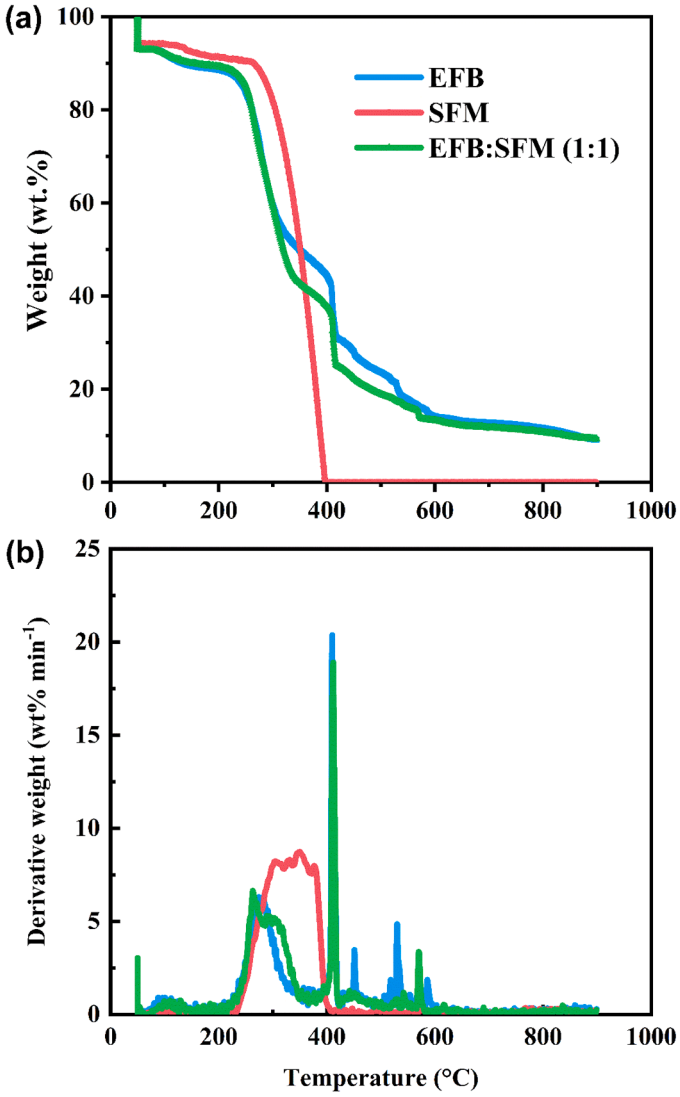

Fig. 1. (a) TGA and (b) DTG curves for EFB, SFM and its mixtures.

3. Results and discussion

3.1. Feedstock characterisation: proximate and ultimate analysis

Table 3 shows the results for ultimate, and proximate analyses of the feedstock samples EFB and SFM. The results are coherent with the findings in literature [63-65]. The moisture content in EFB is determined at 8.8 wt.%. Conversely, SFM do not retain any moisture in atmospheric conditions. Moisture content in the feedstock is undesirable as it would increase the water content of the pyrolytic oil, leading to a decrease in fuel properties [66]. Hence, drying as a pre-treatment process would increase the operational cost of the upscaled pyrolysis process [7]. Following this, the volatile content of EFB and SFM are 72.08 and 97.21 wt.%, respectively. The volatile content could indicate the capacity of fuel readily able to be converted into pyrolytic oil or gas [67]. Furthermore, the fixed carbon and ash content for EFB is 15.90 wt.%, and 3.22 wt.%, respectively. The high fixed carbon and ash content of EFB is undesirable, as it could contribute to the char yield. However, SFM have a significantly lower fixed carbon and ash content of 2.56 and 0.23 wt.%.

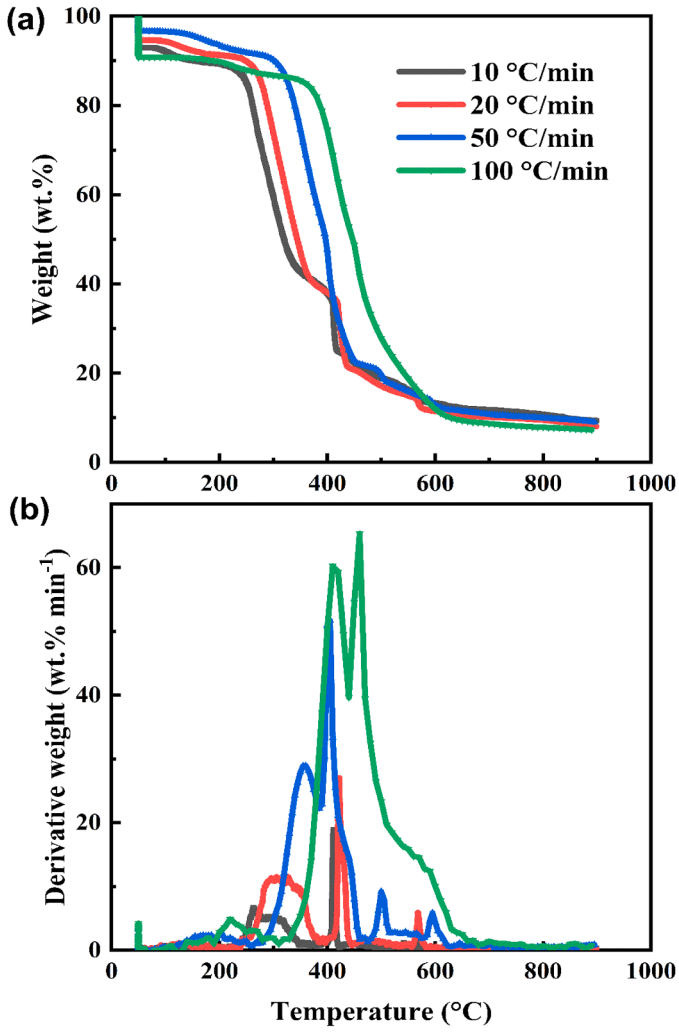

Fig. 2. (a) TGA and (b) DTG curves on the effect of heating rate for EFB:SFM (weight ratio of 1:1).

Additionally, the results from the ultimate analysis showed high oxygen content of EFB, 49.88 wt.%; while SFM do not contain any oxygen content. The high oxygen content in the pyrolytic oil causes thermal instability, which results in a low-quality oil, i.e. having low calorific value, high viscosity, a short shelf life and is corrosive [68]. In contrast, SFM have a higher carbon (84.63 wt.%) and hydrogen content (15.18 wt.%), than EFB (44.82 wt.% and 5.23 wt.%, respectively). The high hydrogen content of SFM could function as a hydrogen pool, donating its hydrogen to stabilise the radical biomass intermediates in the co-pyrolysis process [69].

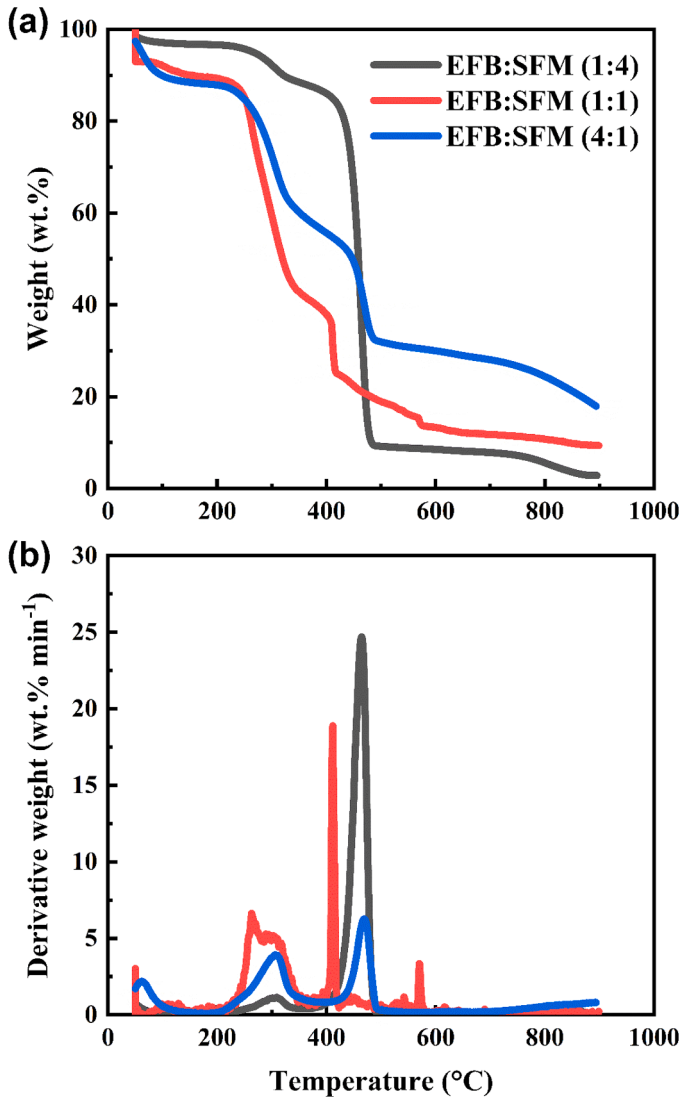

Fig. 3. **(a)** TGA and **(b)** DTG curves of EFB-SFM co-pyrolysis blending ratios.

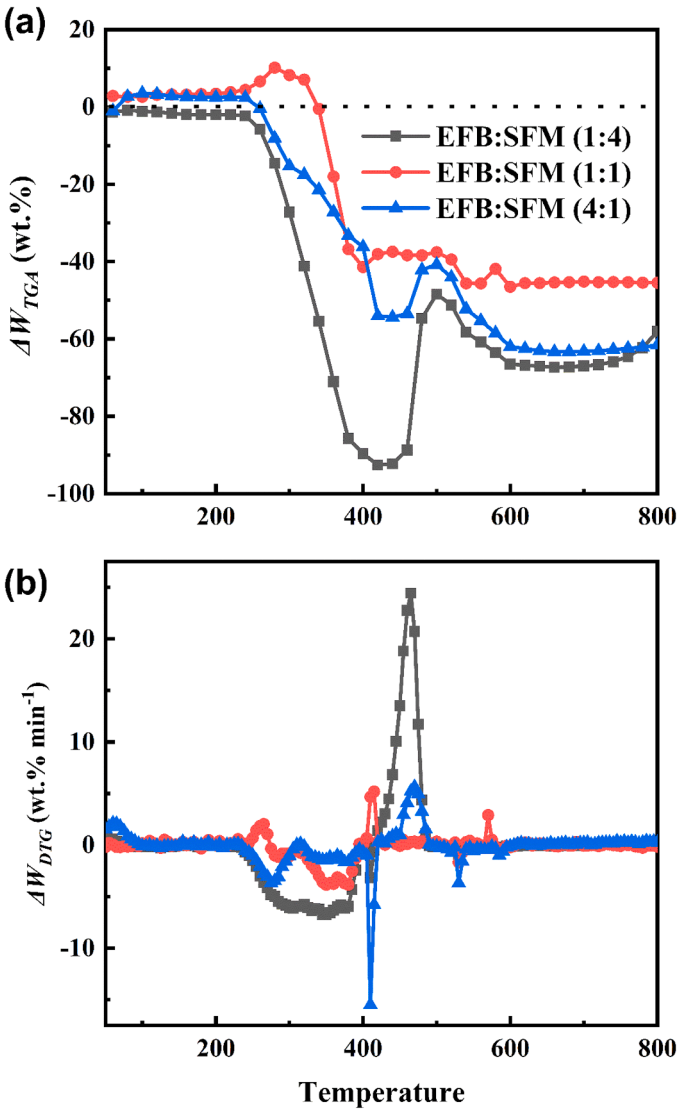

Fig. 4. Synergistic effect of EFB:SFM in terms of **(a)** ΔW_{TGA} and **(b)** ΔW_{DTG}.

3.2. *Thermogravimetric analysis (TGA) and pyrolytic behaviour*

3.2.1. *TGA of EFB and SFM, and its mixtures (1:1)*

Fig. 1 shows the thermogravimetric (TG) curve and derivative thermogravimetric (DTG) curves of pure EFB, pure SFM, and the binary mixture of EFB and SFM in weight ratio of 1:1 at a heating rate of 10 °C. min^{-1}. For the case of thermal degradation of pure EFB, the thermal decomposition starts with moisture removal stage from 64 °C to 172 °C, followed by the main thermal decomposition stages. The reaction thermal decomposition can be divided into two stages for EFB, which consist of (i) the depolymerization of cellulose and hemicellulose at the temperature range from 226 °C to 351 °C, and (ii) devolatilization of lignin at the temperature range from 397 °C to 425 °C. Lignin has a much complex structure than cellulose and hemicellulose, hence, in most TGA studies on biomass feedstock, lignin is often identified as the second peak [70]. At the end of the TGA, the EFB sample achieved a conversion of 90.89 wt.%.

In contrast, the devolatilization process of SFM showed one degradation peak, at the temperature range between 241 °C and 385 °C. Unlike EFB, no significant weight loss was observed below this range due to the absence of moisture content in the SFM sample. The SFM samples achieved complete conversion at the temperature of 385 °C. In comparison to the TGA studies on pure plastic waste feedstocks, the degradation temperature range of LDPE (420 °C - 520 °C) and PP (420 °C - 500 °C) are much higher than the SFM in this current study, albeit the experiment was conducted at a higher heating rate of 20 °C min^{-1} [17]. However, a similar study conducted on the TGA of SFM, reported that at the temperature range of 300 °C to 500 °C, SFM obtained a conversion rate of 97.4 wt.%, which is in better agreement to the current study [71].

Furthermore, for the sample mixture of EFB and SFM (weight ratio of 1:1), the TG curve followed a similar degradation trend as the pure EFB sample, where two distinct peaks were observed. In contrast, the DTG curve showed a broader temperature range at the initial degradation stage of 227 °C to 366 °C, where it is identified that the degradation of the hemicellulose and cellulose from the EFB and SFM component overlapped with each other. The second peak is comparable to that of the second degradation peak of EFB. Additionally, as the SFM component decomposes between the decomposition of cellulose-hemicellulose matrix and lignin, it is possible to overlap with the degradation of lignin as well. Hence this mechanism allows the pyrolysates from the two feedstocks to interact with each other. In similar studies, i.e. the co-pyrolysis of oil palm trunk and PP, three main peaks were observed, where the first peak corresponds to the hemicellulose and cellulose decomposition at 187 °C to 387 °C, which agrees in this current study. Following this, a sharp peak observed in the range from 387 °C to 507 °C which is attributed to the decomposition of the PP material overlapping

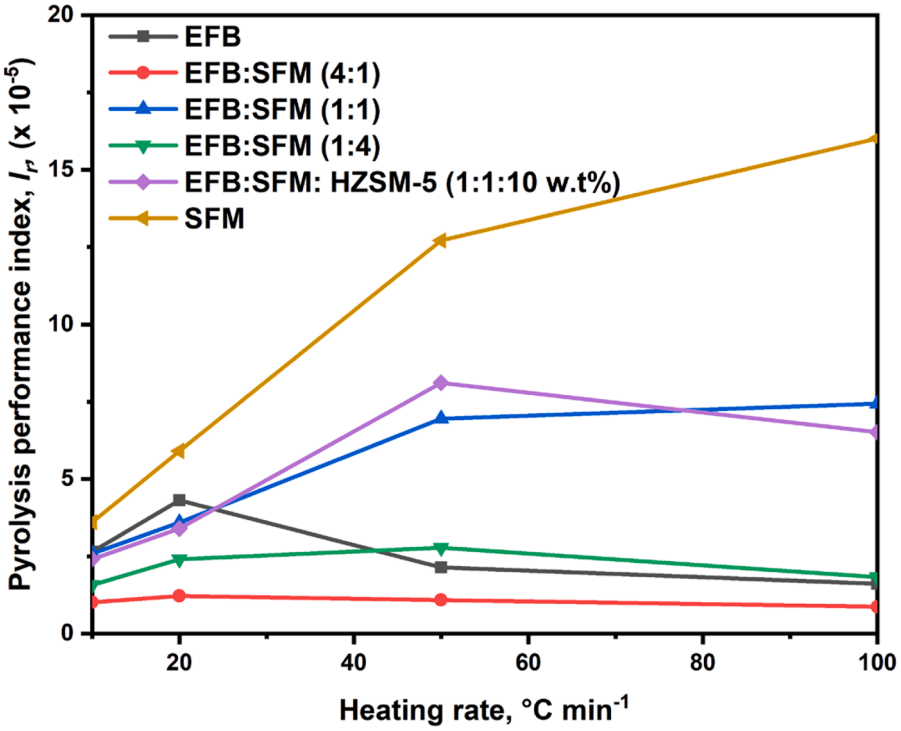

Fig. 5. Pyrolysis performance index trends across different samples and conditions.

Table 4
Thermal degradation of sample mixtures at different heating rates ranging from 10 to 100 °C.min^{-1}.

Sample	Heating rate, °C.min^{-1}	Degradation temperature, °C						Residual weight, wt.%	Peak degradation rate, wt.% min^{-1}	Peak degradation rate, wt.% min^{-1}	I_r (× 10^{-5})	I_r (× 10^{-5})	Average I_r (× 10^{-5})
		Stage 1			Stage 2				Stage 1	Stage 2	Stage 1	Stage 2	
		T_i	T_p	T_f	T_i	T_p	T_f						
EFB	10	226	274	351	397	410	425	9.112	6.294	20.367	2.62	2.68	2.65
	20	230	300	358	386	414	454	12.842	15.285	26.877	5.39	3.23	4.31
	50	245	345	400	415	430	570	12.251	52.536	33.845	1.36	2.92	2.14
	100	350	400	450	460	470	700	10.420	89.575	33.249	1.27	1.97	1.62
SFM	10	241	317	385	–	–	–	0.000	10.022	–	3.60		3.60
	20	262	394	396	–	–	–	0.000	24.147	–	5.91		5.91
	50	310	445	475	–	–	–	0.661	83.819	–	12.71		12.71
	100	380	520	540	–	–	–	0.947	172.508	–	16.01		16.01
EFB:SFM (1:4)	10	194	310	365	377	464	515	2.820	1.139	24.698	0.50	2.66	1.58
	20	251	312	352	401	473	517	9.380	0.866	20.113	0.28	4.53	2.41
	50	258	328	278	438	495	528	7.672	1.053	20.761	0.41	5.14	2.78
	100	287	347	377	407	501	557	6.36	1.083	18.217	0.27	3.38	1.83
EFB:SFM (1:1)	10	227	264	366	400	412	421	9.347	6.538	18.891	2.70	2.47	2.59
	20	230	306	386	400	422	448	8.059	11.513	26.992	3.90	3.28	3.59
	50	255	350	400	400	400	450	9.040	28.925	51.715	7.37	6.53	6.95
	100	310	410	440	450	460	600	7.304	60.258	65.351	9.99	4.88	7.44
EFB:SFM (4:1)	10	190	309	360	416	469	506	17.920	3.905	6.264	1.52	0.52	1.02
	20	200	315	400	448	479	573	17.520	4.064	6.491	1.33	1.10	1.22
	50	208	331	400	420	493	620	23.979	4.248	5.816	1.17	1.00	1.09
	100	218	342	430	440	501	605	25.068	4.211	5.109	0.98	0.76	0.87
EFB:SFM: HZSM-5 (1:1:10 wt)	10	228	288	335	403	414	424	16.641	5.284	19.453	2.24	2.57	2.41
	20	236	320	388	408	426	444	17.410	12.047	24.873	3.81	2.98	3.40
	50	255	345	350	355	380	450	19.125	28.784	51.548	8.50	7.71	8.11
	100	340	420	450	455	460	510	17.410	53.657	61.154	7.73	5.30	6.52

the holocellulose composition. At the end temperature arrange of 800 °C to 900 °C, there was a minor peak, which accounts to the degradation of lignin from the biomass [52].

3.2.2. *Effect of heating rate on the co-pyrolysis of EFB and SFM*

Another observation from the results, is where at greater heating rates the peak temperature is shifted to the right-hand side of the TGA and DTG curves, taking the example of the TGA and DTG curves of the mixed waste thermal decomposition as shown in Fig. 2. This phenomenon is widely referred as thermal lag. As heating rate of the pyrolytic condition increases, the heat transfer to the inner core of the sample particles is limited by the poor thermal conductivity characteristics of

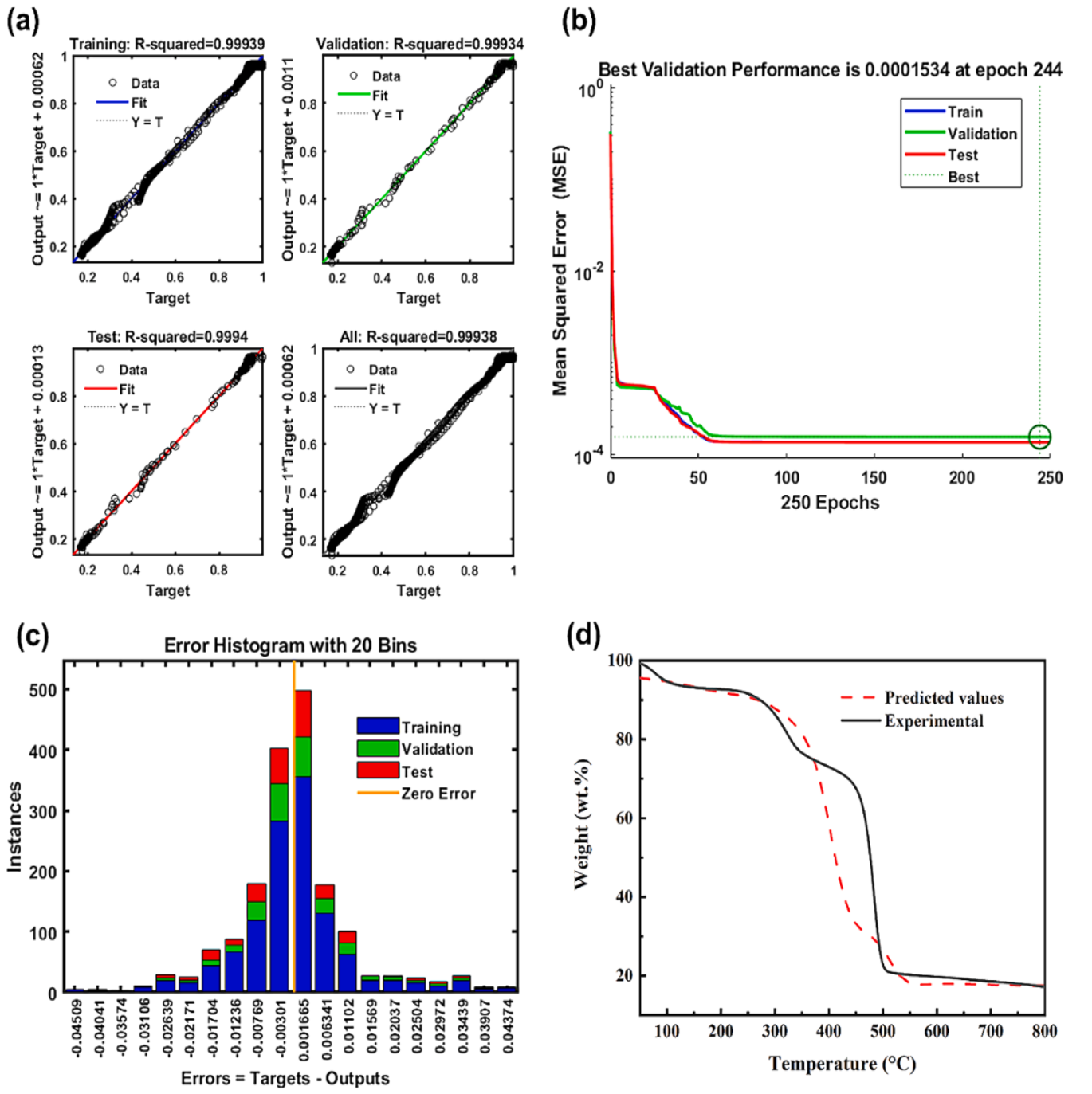

Fig. 6. (a) Regression of the training, validation, and test phase of the ANN model. (b) Minimum MSE obtained at 244th epoch. (c) The normal distribution of the zero error values of the ANN model. (d) ANN model prediction value and the experimental data at CCP of EFB and SFM at 30 °C.min^{-1}.

the biomass and plastic waste sample [15,45]. At a heating rate of 10 °C. min^{-1}, the thermal degradation of the holocellulose component reaches its first peak temperature at 264 °C, whereas at a heating rate of 100 °C. min^{-1}, the initial peak temperature rises to 410 °C. According to Embaye et al. [72], although with elevated heating rates lead to prolonged decomposition attributed by the poor heat transfer, it enhances the degradation rate profiles, which indicates a much rapid decomposition of the feedstock components. In this study, the weight loss rate of the two peaks increases along with heating rate, from 6.538 wt.% min^{-1} and 18.891 wt.%.min^{-1} at 10 °C min^{-1} heating rate, to 60.258 wt.%. min^{-1} and 65.351 wt.% min^{-1} at 100 °C.min^{-1}, this trend also aligns well with other studies [45,73]. At higher heating rates i.e. fast pyrolysis setting, leads to reduced secondary reactions, with more rapid decomposition of fuel components and reduced char products [72]. Based on Table 3, shows the TGA further details the effect of heating rates on the EFB and SFM co-pyrolysis configurations. Throughout the heating rates from 10 to 100 °C.min^{-1}, all results suggest that as heating rate increases, the weight loss rate increases, hence improving the pyrolysis performance index, which will be further detailed in Section 3.2.4.

3.2.3. *Effect of different blending ratio on the co-pyrolysis of EFB and SFM*

Fig. 3 depicts the TG and DTG curves for the co-pyrolysis of EFB and SFM at different mixture ratios, 1:4, 1:1, and 4:1. From the TGA graphs, all mixture ratios result in two main reaction decomposition stages, but in different magnitude in terms of degradation rate. For the case of

Table 5
Kinetic analysis from various samples involved using DAEM.

Sample	α	R^2	Fitted equation	E (kJ mol^{-1})		A (min^{-1})	
				Individual	Average	Individual	Average
EFB	0.2	0.9879	$y = -5552.9\,x + 0.2103$	46.17	79.75	3.73×10^3	1.52×10^8
	0.3	0.9744	$y = -6188.6\,x + 0.9665$	51.45		8.86×10^3	
	0.4	0.9629	$y = -7192.1\,x + 2.3014$	59.79		3.91×10^4	
	0.5	0.8421	$y = -10{,}696\,x + 6.4304$	88.93		3.61×10^6	
	0.6	0.9505	$y = -15{,}092\,x + 11.594$	125.47		8.92×10^8	
	0.7	0.8293	$y = -12{,}833\,x + 7.6261$	106.69		1.43×10^7	
	0.8	0.4518	$y = -11{,}281\,x + 7.6863$	93.79		1.34×10^7	
SFM	0.2	0.9892	$y = -3212.2$ x - 4.2683	26.71	32.22	1.24	1.18×10^2
	0.3	0.9951	$y = -3591.8$ x - 3.8571	29.86		41.3	
	0.4	0.9933	$y = -3670.2$ x - 3.904	30.51		40.3	
	0.5	0.9952	$y = -3962.2$ x - 3.5736	32.94		60.5	
	0.6	0.9962	$y = -4219.5$ x - 3.2938	35.08		85.3	
	0.7	0.9965	$y = -4548.2$ x - 2.9208	37.81		251.0	
	0.8	0.9934	$y = -4874.5$ x - 2.5443	40.53		209.0	
	0.9	0.9910	$y = -5259.5$ x - 2.106	43.73		349.0	
EFB:SFM (1:4 wt.%)	0.2	0.9957	$y = -5424.6$ x - 1.6157	45.10	59.51	1.49×10^4	3.56×10^4
	0.3	0.9608	$y = -5965.9$ x - 1.1675	51.69		1.09×10^4	
	0.4	0.9886	$y = -6217.4$x - 1.1009	49.59		9.77×10^3	
	0.5	0.9943	$y = -7203\,x + 0.0524$	59.89		4.13×10^3	
	0.6	0.9859	$y = -8137\,x + 1.1374$	67.65		1.38×10^4	
	0.7	0.9638	$y = -10{,}001\,x + 3.3809$	83.15		1.60×10^5	
	0.8	0.9713	$y = -10{,}543\,x + 4.0095$	87.65		3.17×10^5	
EFB:SFM (1:1 wt.%)	0.2	0.9945	$y = -5082$ x - 0.7036	42.25	62.71	1.37×10^3	1.45×10^7
	0.3	0.9937	$y = -5337.5$ x - 0.6124	44.38		1.58×10^3	
	0.4	0.9932	$y = -5888.3$ x - 0.0339	48.95		3.10×10^3	
	0.5	0.9903	$y = -6192.6\,x + 0.0569$	51.49		3.57×10^3	
	0.6	0.856	$y = -9063.7\,x + 3.6007$	75.36		1.81×10^5	
	0.7	0.9733	$y = -13{,}692\,x + 9.3587$	113.84		8.65×10^7	
	0.8	0.6830	$y = -12{,}990\,x + 6.6923$	108.00		5.70×10^7	
EFB:SFM (4:1 wt.%)	0.2	0.9803	$y = -7615.4\,x + 4.5634$	63.31	63.92	3.98×10^5	1.12×10^5
	0.3	0.9675	$y = -7158.2\,x + 2.8293$	43.52		4.83×10^4	
	0.4	0.9929	$y = -5235.2$ x - 1.1316	59.51		1.21×10^4	
	0.5	0.9866	$y = -7406\,x + 1.2485$	61.57		1.41×10^4	
	0.6	0.9753	$y = -9854.4\,x + 3.5634$	81.93		1.89×10^5	
	0.7	0.5461	$y = -8858.6$x + 0.9937	73.65		1.30×10^4	
EFB:SFM: HZSM-5 (1:1:10 wt.%)	0.2	0.9763	$y = -4710.6$ x - 1.3702	39.16	56.74	6.52×10^2	2.49×10^5
	0.3	0.9733	$y = -4959.8$ x - 1.2761	41.24		7.54×10^2	
	0.4	0.9671	$y = -5261.7$ x - 1.1039	43.75		9.50×10^2	
	0.5	0.8147	$y = -6481.6\,x + 0.3585$	53.89		5.05×10^3	
	0.6	0.3896	$y = -8344.2\,x + 2.164$	69.37		3.95×10^4	
	0.7	0.9237	$y = -11{,}191\,x + 5.2268$	93.04		1.14×10^6	
	0.8	0.6963	$y = -12{,}233\,x + 4.4367$	101.71		5.63×10^6	

higher composition of SFM (EFB to SFM ratio of 1:4), the first peak (190 °C – 366 °C), which corresponds to the degradation of SFM, cellulose, and hemicellulose is the lowest, with a degradation rate of 1.14 wt.%.min^{-1}. Interestingly, the 1:1 wt ratio showed highest degradation rate activity in the first peak, followed by the blending ratio of EFB to SFM of 4:1 (3.91 wt.%.min^{-1}). In contrast, the following peak (377 °C to 515 °C), the degradation rate increases as SFM composition increases, which peaked at the mixture ratio of EFB to SFM of 1:4, with a degradation rate of 24.70 wt.%.min^{-1}.

In addition, to determine if the EFB and SFM samples exhibit any synergistic or inhibitory relationship, the TG and DTG difference between experimental and theoretical, ΔW_{TGA} and ΔW_{DTG} was calculated across the heating temperature of 50 to 800 °C. Among the mixture ratio TGA experiments conducted, Fig. 4**(a)** shows that only at mixture ratio of EFB to SFM 1:1, positive synergy at the temperature range of 180 °C to 320 °C was observed. This temperature range coincide with the degradation of SFM, hemicellulose, and cellulose, with a maximum difference of 10.15 wt.% at 280 °C. Hence, the synergy at SFM:EFB 1:1 showed that there was sufficient amount of hydrogen donating plastic constituents, to react and stabilises biomass radicals, thus contributes to a greater degradation rate [74]. However, it is followed by a negative dip at 320 °C. The thermal degradation behaviour of the co-pyrolysis of EFB and SFM is predominantly inhibitory, where experimental values are higher than the theoretical values. The negative synergistic effect could be explained by the heterogenous mixture of the EFB and SFM mixtures causing a local heat transfer limitation in the matrix [75], which was also reported in the study of agricultural biomass and polyolefin plastic co-pyrolysis [17]. In a different perspective, the mass loss rate difference in Fig. 4**(b)** depicts the ΔW_{DTG} across the different blends of EFB and SFM mixture. The positive values of the ΔW_{DTG} indicates a synergistic relationship. Conversely, this would be an inhibitory relationship. From the results, temperature range before 418 °C showed negligible or negative values (237 °C – 396 °C) for ΔW_{DTG}. However, the ΔW_{DTG} shifted to a positive value in the range of 418 °C to 500 °C. This observation agrees with [17], where the co-pyrolysis of HDPE with biomass blends showed a positive synergy in the range of 450 °C to 520 °C. According to Salvilla et al. [17], this inhibitory relationship followed by a promotional effects' phenomenon can be attributed to the volatiles being trapped in the melt phase of the plastic component. This inhibits the mass loss rate at the lower temperature showing an inhibitory effect. As the temperature elevated, the release of these trapped volatiles contributed to the increase in mass loss rate.

3.2.4. *Pyrolysis performance study*

Moreover, the pyrolysis performance index, I_r was calculated to evaluate the pyrolytic behaviour of the feedstock samples. Firstly, the initial temperature of the degradation peak, T_i, the final temperature of the degradation peak, T_f, the degradation peak temperature, T_p, the maximum weight loss rate, and the residual weight of all the sample mixtures with varying heating rate were identified and summarized in

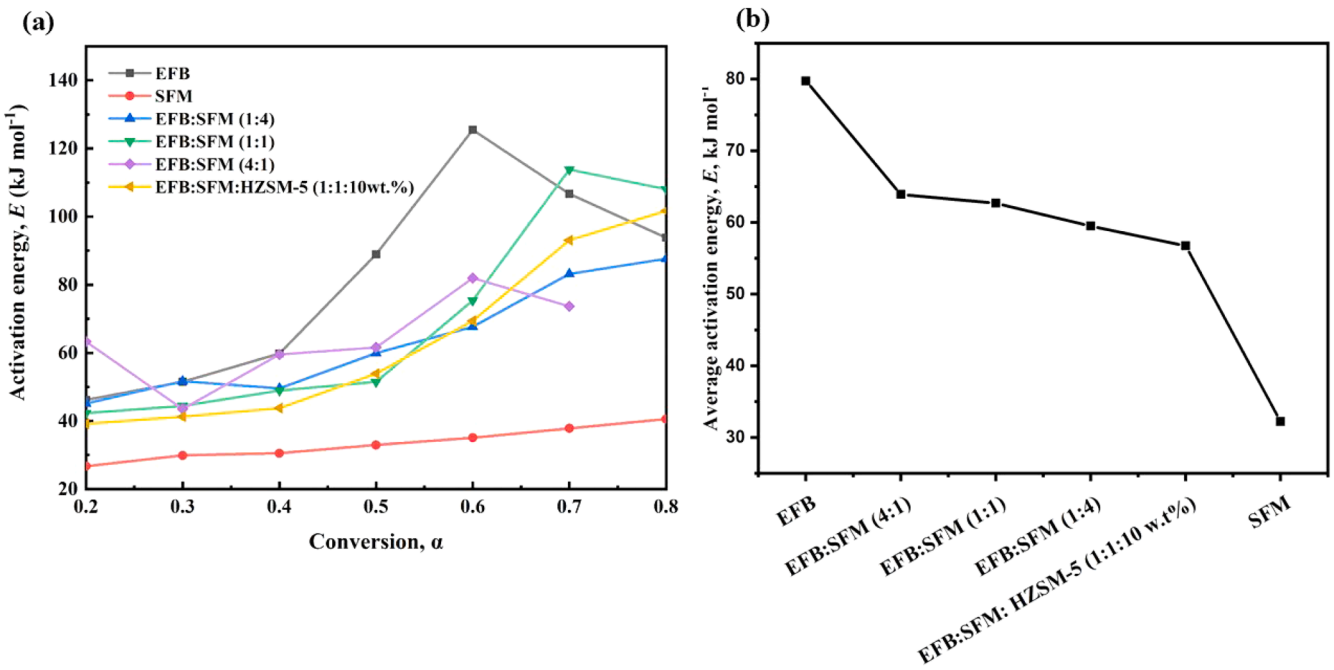

Fig. 7. (a) *E* trends across conversion rate between different samples and mixtures, (b) average *E* trends across different samples and mixture ratio.

Fig. 5, Table 4. The EFB showed comparable results as heating rate increased, indicating that the reaction is independent of heating rate. This may be attributed by the high lignin content in EFB, which the end products are the biochar, lowering the conversion rate [76]. In the case of co-pyrolysis system, the addition of the SFM enhanced the overall I_r of EFB at all heating rates experiment. The reaction time is shortened, and the maximum degradation rates have increased, thus improving the pyrolysis reaction. With the addition of a catalyst, the results were comparable results, with the best recorded I_r value of 8.11 obtained from HZSM-5 catalyst at heating rate of 50 °C.min^{-1}.

3.3. Model fitting with artificial neural network (ANN)

An ANN model was constructed to model-fit the CCP of EFB and SFM behaviour. The ANN model was built with the reaction temperature (50 °C to 800 °C) and heating rates (10, 20, 50, and 100 °C.min^{-1}) as the input variables and the corresponding weight ratio as the output variable. Fig. 6**(a)** and **(b)** shows the performance of the trained ANN model. The regression (R^2) and the mean square error (MSE) obtained from the training, was 0.9939, and 1.534 × 10^{-4} (at the 244th epoch), respectively. Besides that, Fig. 6**(c)** also shows the error histogram is normally distributed throughout the zero error, between the values −0.045 and 0.044. Hence, this performance demonstrates that the differences between the target and output values are not significant, indicating a well-trained network. Fig. 6**(d)** showed a sample prediction for the CCP of EFB and SFM at 30 °C min^{-1} heating rate, where the experimental data were not included in the training of the ANN model. The results showed some discrepancy. However, it was able to predict the general thermal degradation pattern and was able to predict the residual weight accurately. The performance for the prediction against the experimental result was R^2 of 0.9295 and a MSE of 9.34 × 10^{-3}.

3.4. Thermo-kinetic analysis

3.4.1. Kinetic analysis using DAEM method

The TGA experimental data showed good linear fit for all the single feedstock and binary feedstock blends, in the **Supplementary materials,** with regression coefficients (R^2), greater than 0.8 for all conversion range of 0.1–0.8. However, at $\alpha = 0.1$, this region often refers to the dewatering process in the biomass composition, where it causes discrepancies in the results. Hence the low R^2 values. Besides that, at $\alpha = 0.8$, where this region corresponds to the degradation of the recalcitrant lignin component, would also reduce the accuracy of the model. Therefore, in this study, the DAEM for EFB and its mixtures will only cover the conversion range of α = 0.2 to 0.7, for the computation of kinetic parameters, while pure SFM is conducted in its full conversion range. By taking the average *E* and *A* of each stepwise conversion of α = 0.1. the average values of *E* and *A* for the single feedstock EFB were determined at 79.75 kJ.mol^{-1} and 1.52 × 10^8 min^{-1}, respectively (Table 5). The results are in agreement with the study conducted by Sidek et al. [77], where the *E* and *A* parameters determined *via* Criado method of the 3rd order, was 76.53–77.19 kJ.mol^{-1} and 1.07–1.62 × 10^4 min^{-1}, respectively. In contrast, Surahmanto et al. [78], determined the *E* and *A* parameters by DAEM method, 107–18 – 227.28 kJ.mol^{-1} and 1.79 × 10^{13} – 9.87 × 10^{20} s^{-1}, respectively. The ambiguous results for the activation energy arise due to the difference in the organic constituent's present [79]. While for SFM, the values are 32.22 kJ.mol^{-1} and 1.18 × 10^2 min^{-1}, respectively. However, the thermo-kinetic parameters reported by Montero-Calderón et al. [80], determined a greater value of *E* and *A*, 182.23 - 214.80 kJ.mol^{-1} and 3.70 × 10^{11} – 1.50 × 10^{16} s^{-1}, respectively. The higher *E* from biomass attributes t the thermal stability properties of lignocellulosic constituents as observed in the TGA studies in Section 3.2.1. In contrast, SFM made from polyolefin materials are easily volatised.

Fig. 7**(a)** highlights the *E* distribution for each conversion step where *E* was observed to be on the higher side as the conversion rate progresses, especially samples with EFB. This trend was also in agreement with a study conducted on the co-pyrolysis of non-edible seeds with LDPE waste from Mohan et al. [39], and the *E* distribution of pine wood and corn straw from Mian et al. [81]. At $\alpha < 0.5$ for the pure EFB sample, the *E* are low at the range of 41.77 - 59.79 kJ mol^{-1}, which attributes to the energy required to decompose cellulose and hemicellulose. While at $\alpha > 0.5$, the *E* required increased significantly to 88.93 - 125.47 kJ mol^{-1}, which indicates most of the hemicellulose and cellulose had been decomposed, and a higher energy requirement is needed to thermally degrade lignin. On the contrary, the *E* throughout the thermal conversion of SFM is identical, indicating a homogenous plastic sample.

Table 6
Thermodynamic analysis from various samples involved.

Sample	α	ΔH (kJ.mol^{-1})		ΔG (kJ.mol^{-1})		ΔS (kJ.mol^{-1}.K^{-1})	
		Individual	Average	Individual	Average	Individual	Average
EFB	0.2	41.28	74.30	152.98	169.73	−0.1900	−0.1484
	0.3	46.43		156.88		−0.1831	
	0.4	54.66		160.20		−0.1709	
	0.5	83.36		173.16		−0.1340	
	0.6	119.56		182.56		−0.0887	
	0.7	100.49		192.58		−0.1234	
	0.8	86.86		190.94		−0.1249	
SFM	0.2	21.46	26.71	168.36	176.18	−0.2324	−0.2261
	0.3	24.48		172.30		−0.2283	
	0.4	25.01		176.40		−0.2287	
	0.5	27.36		178.62		−0.2254	
	0.6	29.43		180.68		−0.2227	
	0.7	32.09		179.14		−0.2138	
	0.8	34.75		184.47		−0.2154	
	0.9	37.88		186.44		−0.2112	
EFB:SFM (1:4 wt.%)	0.2	39.41	53.46	162.57	184.33	−0.1798	−0.1799
	0.3	45.81		175.01		−0.1827	
	0.4	43.55		177.12		−0.1838	
	0.5	53.75		194.94		−0.1911	
	0.6	61.42		197.10		−0.1812	
	0.7	76.83		199.24		−0.1609	
	0.8	81.29		200.05		−0.1553	
EFB:SFM (1:1 wt.%)	0.2	37.37	57.37	153.75	168.08	−0.1984	−0.1744
	0.3	39.35		158.88		−0.1975	
	0.4	43.77		163.37		−0.1921	
	0.5	46.14		169.25		−0.1912	
	0.6	69.69		178.09		−0.1590	
	0.7	107.90		185.16		−0.1081	
	0.8	101.61		202.47		−0.1313	
EFB:SFM (4:1 wt.%)	0.2	58.69	58.34	142.46	173.08	−0.1508	−0.1704
	0.3	38.60		138.53		−0.1688	
	0.4	54.24		169.01		−0.1809	
	0.5	55.87		179.50		−0.1803	
	0.6	75.76		193.97		−0.1593	
	0.7	66.89		215.03		−0.1823	
EFB:SFM: HZSM-5 (1:1:10 wt.%)	0.2	34.20	51.25	156.39	170.51	−0.2047	−0.1887
	0.3	36.12		161.67		−0.2037	
	0.4	38.47		166.83		−0.2021	
	0.5	48.40		172.76		−0.1885	
	0.6	63.50		185.03		−0.1720	
	0.7	86.82		194.89		−0.1445	
	0.8	94.66		222.96		−0.1514	

For biomass-plastic waste matrix, it was obvious the E required for the thermal conversion increases, as EFB composition increases (Fig. 7 **(b)**). Taking the mixture ratio 1:1 as an example, the E obtained from the experimental data was 62.71 kJ.mol^{-1}, while theoretically, by taking the average E from the single feedstock analysis, it would only require 55.99 kJ.mol^{-1}. This could very well contribute by the negative synergy between both samples due to their heterogenous nature [75]. To overcome this limitation, catalytic co-pyrolysis with HZSM-5, showed that the overall E across conversion rate is lower than that of single feedstock EFB and the co-feedstock matrix without catalyst, thus implied a much energy efficient configuration.

3.4.2. *Thermodynamic analysis*

Table 6 summarises the thermodynamic parameters such as ΔH, ΔG, and ΔS, at each α values. The ΔH refers to the energy difference between the reactant and products, it is an indicator whether a reaction is endothermic or exothermic in nature. From the results, the ΔH values for all samples and its mixtures are positive, which means that the pyrolysis, and co-pyrolysis process in general is endothermic. Furthermore, according to Jung et al. [32], if the deviation between the average ΔH and the average E values is <7 kJ.mol^{-1}, it signifies that the thermal decomposition reaction is likely to take place. From the current study, the difference between the ΔH and E for the samples and its mixtures ranges between 5.34 to 5.51 kJ.mol^{-1}, indicating the pyrolysis reaction is expected to occur. Furthermore, in comparison to the ΔH values between the single feedstock pyrolysis of EFB and co-pyrolysis of EFB-SFM blends, the latter showed a reduction in ΔH of 21.48 % to 28.05 % (between the EFB-SFM blends of 4:1, 1:1, and 1:4). Following this, with an addition of HZSM-5 catalyst, the thermal requirement was further reduced by 10.67 % (as compared to EFB-SFM = 1:1 blend co-pyrolysis). This implies that, the system becomes less endothermic, which allows the reaction to occur at a much lower thermal requirement.

Following this, ΔG describes the increase in the total energy of the system, in the process of formation of co-pyrolysis complex [55,72]. A positive ΔG signifies the system is thermodynamically challenged and non-spontaneous [55]. In this study, the average ΔG of all pyrolysis, co-pyrolysis, and catalytic co-pyrolysis reaction revealed positive values ranging from 168.08 kJ.mol^{-1} to 184.33 kJ.mol^{-1}. This means that the reaction is highly unfavourable thermodynamically. Although the average ΔG does not show any significant trends, individual thermal degradation follows an increase in ΔG with each conversion step, α.

Moreover, ΔS reflects the degree of disorder of a reaction system [32]. Lower or negative ΔS values indicates that the system had attained thermodynamic equilibrium from going through physicochemical changes. While positive and high values of ΔS means that the reaction system is far from thermodynamic equilibrium. To demonstrate, the ΔS negative values computed in this study indicates that formation of thermodynamically more stable products from the starting reactants [82]. Besides that, from the individual thermal decomposition results, as

higher conversion is achieved, the ΔS value also increases, which indicates that the reactivity of the system had also increased. This finding agreed with [55], which further explain that the reaction modules reacted faster to generate an activated complex at reduced residence times.

4. Conclusion

In summary, the co-pyrolysis relationship between EFB and SFM, and the presence of a catalyst (HZSM-5) have been studied at varying heating rates of 10–100 °C.min^{-1}. Higher degradation rate was found in higher heating rate. At heating rate of 100 °C.min^{-1}, the degradation rate was reported at 65.351 wt.%.min^{-1}. Meanwhile, at heating rate of 10 °C.min^{-1}, the degradation rate was found 18.891 wt.%.min^{-1}. Furthermore, the pyrolysis performance index, I_r, which measures the pyrolytic efficiency of the sample matrix was evaluated. At heating rate of 10 °C.min^{-1}, the I_r found was 2.59. Meanwhile, at heating rate of 100 °C.min^{-1}, the I_r value increased to 7.44. Moreover, the role of the HZSM-5 catalyst was significant, where at heating rate of 50 °C.min^{-1}, the highest average I_r value of 8.11 was achieved. Furthermore, the reaction kinetics via the DAEM method showed good linearity of $R^2 > 0.80$. Notably, the values of E and the ΔH of the EFB-SFM blends showed reduction of 21.37 % and 22.79 %, respectively, as compared to the single feedstock EFB pyrolysis. Furthermore, the E and the ΔH parameters showed a further reduction of 13.54 % and 14.94 %, respectively with HZSM-5 catalyst. The enhancement of the I_r and the reduction of reaction energy requirement with HZSM-5 catalyst, shows that the selection of an effective catalyst is imperative in the design of a more energy efficient reactor system. Future studies can explore different catalyst design to further enhance the energy efficiency and green fuel production rate. Following this, the thermo-kinetic parameters determined from this work presents the catalytic co-pyrolysis of SFM and EFB with HZSM-5 catalyst has the potential as feedstocks for fuel generation, while addressing the hazardous issues associated with SFM. Moreover, the demonstration of the ANN model in recognising the catalytic co-pyrolysis behaviour of the EFB-SFM mixtures could help in predicting the outcome of different input parameter configurations improving the efficiency of not requiring additional laboratory experiments. Extended work can be conducted to broaden the ANN model to input additional parameters, i.e. proximate and ultimate analysis results of different biomass-plastic waste samples, such that the prediction model can be robust enough to encompass different co-pyrolysis feedstock combinations.

Data availability

Data will be made available upon request.

CRediT authorship contribution statement

Melvin Xin Jie Wee: Writing – original draft, Methodology, Investigation, Formal analysis, Data curation, Conceptualization. **Bridgid Lai Fui Chin:** Writing – review & editing, Supervision, Resources, Project administration, Investigation, Funding acquisition, Conceptualization. **Agus Saptoro:** Writing – review & editing, Supervision. **Jiuan Jing Chew:** Writing – review & editing, Supervision. **Jaka Sunarso:** Writing – review & editing, Supervision. **Suzana Yusup:** Writing – review & editing, Supervision. **Abhishek Sharma:** Writing – review & editing, Resources, Data curation.

Declaration of competing interest

The authors declare that they have no known competing financial interests or personal relationships that could have appeared to influence the work reported in this paper.

Acknowledgements

The authors would like to appreciate the funding support from JASTIP-Net (Japan-ASEAN Science, Technology and Innovation Platform) 2023/24 on the research project entitled, 'Sustainable Production of Value-Added Products and Energies from Oil Palm Residues and Plastic Waste Mixtures in the ASEAN Region' and also the Institute of Chemical Engineers Palm Oil Processing Special Interest Group (IChemE POPSIG) for the POPSIG Student Research Project Bursary. The authors also would like to acknowledge the technical support from Curtin University Malaysia, Swinburne University of Technology, Universiti Teknologi PETRONAS (UTP), and Manipal University Jaipur. Besides that, M.X.J. Wee would like to acknowledge the full funding support from the Curtin Malaysia Postgraduate Research Studentship (CMPRS) for the PhD study.

Supplementary materials

Supplementary material associated with this article can be found, in the online version, at doi:10.1016/j.jtice.2024.105811.

References

[1] Kahar P, Rachmadona N, Pangestu R, Palar R, Triyono Nugroho Adi D, Betha Juanssilfero A, Yopi IManurung, Hama S, Ogino C. An integrated biorefinery strategy for the utilization of palm-oil wastes. Bioresour Technol 2022;344:126266.
[2] Loh SK. The potential of the Malaysian oil palm biomass as a renewable energy source. Energy Convers Manag 2017;141:285–98.
[3] Foong SY, Chan YH, Lock SSM, Chin BLF, Yiin CL, Cheah KW, Loy ACM, Yek PNY, Chong WWF, Lam SS. Microwave processing of oil palm wastes for bioenergy production and circular economy: recent advancements, challenges, and future prospects. Bioresour Technol 2023;369:128478.
[4] Chin BLF, Gorin A, Chua HB, Twaiq F. Experimental investigation on tar produced from palm shells derived syngas using zeolite HZSM-5 catalyst. J Energy Inst 2016;89(4):713–24.
[5] Chai YH, Mohamed M, Cheng YW, Chin BLF, Yiin CL, Yusup S, Lam MK. A review on potential of biohydrogen generation through waste decomposition technologies. Biomass Convers Biorefin 2023;13:8549–74.
[6] Haq IU, Qaisar K, Nawaz A, Akram F, Mukhtar H, Zohu X, Xu Y, Mumtaz MW, Rashid U, Ghani WA, Choong TS. Advances in valorization of lignocellulosic biomass towards energy generation. Catalysts 2021;11:309.
[7] Halim SA, Mohd NA, Razali NA. A comparative assessment of biofuel products from rice husk and oil palm empty fruit bunch obtained from conventional and microwave pyrolysis. J Taiwan Inst Chem Eng 2022;134:104305.
[8] Escalante J, Chen W-H, Tabatabaei M, Hoang AT, Kwon EE, Lin K-YAndrew, Saravanakumar A. Pyrolysis of lignocellulosic, algal, plastic, and other biomass wastes for biofuel production and circular bioeconomy: a review of thermogravimetric analysis (TGA) approach. Renew Sustain Energy Rev 2022;169:112914.
[9] Y.H.Chan SSMLock, Chin BLF, Wong MK, Loy ACM, Foong SY, Yiin CL, Lam SS. Progress in thermochemical co-processing of biomass and sludge for sustainable energy, value-added products and circular economy. Bioresour Technol 2023;380:129061.
[10] Ansari KB, Hassan SZ, Bhoi R, Ahmad E. Co-pyrolysis of biomass and plastic wastes: a review on reactants synergy, catalyst impact, process parameter, hydrocarbon fuel potential, COVID-19. J Environ Chem Eng 2021;9:106436.
[11] Engamba Esso SB, Xiong Z, Chaiwat W, Kamara MF, Longfei X, Xu J, Ebako J, Jiang L, Su S, Hu S, Wang Y, Xiang J. Review on synergistic effects during co-pyrolysis of biomass and plastic waste: significance of operating conditions and interaction mechanism. Biomass Bioenergy 2022;159:106415.
[12] Gin AW, Hassan H, Ahmad MA, Hameed BH, Mohd Din AT. Recent progress on catalytic co-pyrolysis of plastic waste and lignocellulosic biomass to liquid fuel: the influence of technical and reaction kinetic parameters. Arab J Chem 2021;14:103035.
[13] Wang Z, Burra KG, Lei T, Gupta AK. Co-pyrolysis of waste plastic and solid biomass for synergistic production of biofuels and chemicals-A review. Prog Energy Combust Sci 2021;84:100899.
[14] Wee MXJ, Chin BLF, Saptoro A, Yiin CL, Chew JJ, Sunarso J, Yusup S, Sharma A. A review on co-pyrolysis of agriculture biomass and disposable medical face mask waste for green fuel production: recent advances and thermo-kinetic models. Front Chem Sci Eng 2023;17:1141–61.
[15] Burra KG, Gupta AK. Kinetics of synergistic effects in co-pyrolysis of biomass with plastic wastes. Appl Energy 2018;220:408–18.
[16] Li J, Yao X, Chen S, Xu K, Fan B, Yang D, Geng L, Qiao H. Investigation on the co-pyrolysis of agricultural waste and high-density polyethylene using TG-FTIR and artificial neural network modelling. Process Saf Environ Protect 2022;160:341–53.

[17] Salvilla JNV, Ofrasio BIG, Rollon AP, Manegdeg FG, Abarca RRM, de Luna MDG. Synergistic co-pyrolysis of polyolefin plastics with wood and agricultural wastes for biofuel production. Appl Energy 2020;279:115668.
[18] Singh S, Tagade A, Verma A, Sharma A, Tekade SP, Sawarkar AN. Insights into kinetic and thermodynamic analyses of co-pyrolysis of wheat straw and plastic waste via thermogravimetric analysis. Bioresour Technol 2022:127332.
[19] Stančin H, Mikulčić H, Manić N, Stojiljković D, Vujanović M, Wang X, Duić N. Thermogravimetric and kinetic analysis of biomass and polyurethane foam mixtures Co-Pyrolysis. Energy 2021;237:121592.
[20] Zheng Y, Tao L, Yang X, Huang Y, Liu C, Zheng Z. Study of the thermal behavior, kinetics, and product characterization of biomass and low-density polyethylene co-pyrolysis by thermogravimetric analysis and pyrolysis-GC/MS. J Anal Appl Pyrolysis 2018;133:185–97.
[21] Tan IJY, Loy ACM, Chin BLF, Cheah KW, Teng SY, How BS, Alhamzi H, Leong WD, Lim HY, Lam MK, Lam SS. Co-pyrolysis of *Chlorella vulgaris* with plastic wastes: thermal degradation, kinetics and Progressive Depth Swarm-Evolution (PDSE) neural network-based optimization. Green Technol Sustain 2024;2:100077.
[22] Ghorbannezhad P, Park S, Onwudili JA. Co-pyrolysis of biomass and plastic waste over zeolite- and sodium-based catalysts for enhanced yields of hydrocarbon products. Waste Manag 2020;102:909–18.
[23] Jin Q, Wang X, Li S, Mikulčić H, Bešenić T, Deng S, Vujanović M, Tan H, Kumfer BM. Synergistic effects during co-pyrolysis of biomass and plastic: gas, tar, soot, char products and thermogravimetric study. J Energy Inst 2019;92:108–17.
[24] Jin X, Lee JH, Choi JW. Catalytic co-pyrolysis of woody biomass with waste plastics: effects of HZSM-5 and pyrolysis temperature on producing high-value pyrolytic products and reducing wax formation. Energy 2022;239:121739.
[25] Stančin H, Šafář M, Růžičková J, Mikulčić H, Raclavská H, Wang X, Duić N. Co-pyrolysis and synergistic effect analysis of biomass sawdust and polystyrene mixtures for production of high-quality bio-oils. Process Saf Environ Protect 2021;145:1–11.
[26] Ullah F, Zhang L, Ji G, Irfan M, Ma D, Li A. Experimental analysis on products distribution and characterization of medical waste pyrolysis with a focus on liquid yield quantity and quality. Sci Total Environ 2022;829:154692.
[27] Xu R, Yan C, Liu Q, Liu E, Zhang H, Zhang X, Yuan X, Han L, Lei H, Ruan R, Zhang X. Development of metal-doping mesoporous biochar catalyst for co-valorizing biomass and plastic waste into valuable hydrocarbons, syngas, and carbons. Fuel Process Technol 2022;227:107127.
[28] Wu M, Wang Z, Chen G, Zhang M, Sun T, Wang Q, Zhu H, Guo S, Chen Y, Zhu Y, Lei T, Burra KG, Gupta AK. Synergistic effects and products distribution during Co-pyrolysis of biomass and plastics. Journal of the Energy Institute 2023;111:101392.
[29] Liang Y, Song Q, Wu N, Li J, Zhong Y, Zeng W. Repercussions of COVID-19 pandemic on solid waste generation and management strategies. Front Environ Sci Eng 2021;15:115.
[30] Patrício Silva AL, Prata JC, Duarte AC, Barcelò D, Rocha-Santos T. An urgent call to think globally and act locally on landfill disposable plastics under and after covid-19 pandemic: pollution prevention and technological (Bio) remediation solutions. Chem Eng J 2021;426:131201.
[31] Patrício Silva AL, Prata JC, Mouneyrac C, Barcelò D, Duarte AC, Rocha-Santos T. Risks of Covid-19 face masks to wildlife: present and future research needs. Sci Total Environ 2021;792:148505.
[32] Jung S, Lee S, Dou X, Kwon EE. Valorization of disposable COVID-19 mask through the thermo-chemical process. Chem Eng J 2021;405:126658.
[33] Lee SB, Lee J, Tsang YF, Kim Y-M, Jae J, Jung S-C, Park Y-K. Production of value-added aromatics from wasted COVID-19 mask via catalytic pyrolysis. Environ Pollut 2021;283:117060.
[34] Yousef S, Eimontas J, Striūgas N, Abdelnaby MA. Pyrolysis kinetic behaviour and TG-FTIR-GC–MS analysis of Coronavirus face masks. J Appl Pyrolysis 2021;156:105118.
[35] Yousef S, Eimontas J, Striūgas N, Abdelnaby MA. A new strategy for butanol extraction from COVID-19 mask using catalytic pyrolysis process over ZSM-5 zeolite catalyst and its kinetic behavior. Thermochim Acta 2022;711:179198.
[36] Dubdub I. Artificial neural network study on the pyrolysis of polypropylene with a sensitivity analysis. Polymers (Basel) 2023;15:494.
[37] Nawaz A, Kumar P. Thermal degradation of hazardous 3-layered COVID-19 face mask through pyrolysis: kinetic, thermodynamic, prediction modelling using ANN and volatile product characterization. J Taiwan Inst Chem Eng 2022;139:104538.
[38] Wang Y, Yang S, Bao G, Wang H. Investigation of tobacco straw pyrolysis: three-parallel Gaussian reaction modeling, products analysis and ANN application. Ind Crops Prod 2023;200:116864.
[39] Mohan I, Panda AK, Mandal S, Kumar S. Co-pyrolysis of Azadirachta indica non-edible seed and waste LDPE: analysis of kinetic models using thermogravimetric analyser and prediction modeling with Artificial Neural Network (ANN). Fuel 2023;350:128765.
[40] Fong MJB, Loy ACM, Chin BLF, Lam MK, Yusup S, Jawad ZA. Catalytic pyrolysis of Chlorella vulgaris: kinetic and thermodynamic analysis. Bioresour Technol 2019;289:121689.
[41] Osman AI, Young TJ, Farrell C, Harrison J, Al-Muhtaseb AaH, Rooney DW. Physicochemical characterization and kinetic modeling concerning combustion of waste berry pomace. ACS Sustain Chem Eng 2020;8:17573–86.
[42] Li M, Liu L, Jiang L, Gou F-H, Sun J-H. Application of distributed activation energy models to polymer pyrolysis: effects of distributed model selection, characteristics, validation, and sensitivity analysis. Fuel 2019;254:115594.
[43] Sfakiotakis S, Vamvuka D. Development of a modified independent parallel reactions kinetic model and comparison with the distributed activation energy model for the pyrolysis of a wide variety of biomass fuels. Bioresour Technol 2015;197:434–42.
[44] Navarro MV, López JM, Veses A, Callén MS, García T. Kinetic study for the co-pyrolysis of lignocellulosic biomass and plastics using the distributed activation energy model. Energy 2018;165:731–42.
[45] Ng QH, Chin BLF, Yusup S, Loy ACM, Chong KYY. Modeling of the co-pyrolysis of rubber residual and HDPE waste using the distributed activation energy model (DAEM). Appl Therm Eng 2018;138:336–45.
[46] Ruiz-Montoya M, Palma A, Lozano-Calvo S, Morales E, Díaz MJ. Kinetic synergistic effect in co-pyrolysis of Eucalyptus globulus with high and low density polyethylene. Energy Rep 2022;8:10688–704.
[47] Anh Vo T, Vu Ly H, Hwang I, Hwang HT, Kim J, Kim S-S. Enhancement of biofuel quality via conventional and catalytic co-pyrolysis of bamboo with polystyrene in a bubbling fluidized bed reactor: coupled experiments and artificial neural network modeling. Fuel 2023;346:128403.
[48] Abdullahi Shagali A, Hu S, Li H, He L, Han H, Chi H, Qing H, Xu J, Jiang L, Wang Y, Su S, Xiang J. Synergistic interactions and co-pyrolysis characteristics of lignocellulosic biomass components and plastic using a fast heating concentrating photothermal TGA system. Renew Energy 2023;215:118936.
[49] Berthold EES, Deng W, Zhou J, Bertrand AME, Xu J, Jiang L, Su S, Hu S, Hu X, Wang Y, Xiang J. Impact of plastic type on synergistic effects during co-pyrolysis of rice husk and plastics. Energy 2023;281:128270.
[50] Su G, Zulkifli NWM, Ong HC, Ibrahim S, Cheah MY, Zhu R, Bu Q. Co-pyrolysis of medical protective clothing and oil palm wastes for biofuel: experimental, techno-economic, and environmental analyses. Energy 2023;273:127221.
[51] Terry LM, Wee MXJ, Chew JJ, Khaerudini DS, Darsono N, Aqsha A, Saptoro A, Sunarso J. Catalytic co-pyrolysis of oil palm trunk and polypropylene with Ni–Mo/TiO2 and Ni/Al2O3: oil composition and mechanism. Environ. Res. 2023;224:115550.
[52] Terry LM, Wee MXJ, Chew JJ, Khaerudini DS, Timuda GE, Aqsha A, Saptoro A, Sunarso J. Co-pyrolysis of oil palm trunk and polypropylene: pyrolysis oil composition and formation mechanism. S Afr J Chem Eng 2023;43:348–58.
[53] Lim HY, Yusup S, Acda MN, Chin BLF, Rianawati E, Unrean P, Yiin CL, Quitain AT, Assabumrungrat S. Investigation of calcium oxide–impregnated zeolite catalyst toward catalytic pyrolysis of oil palm empty fruit bunch: bio-oil yields, characterizations, and kinetic study. Bioenergy Res 2023.
[54] Chee ALK, Chin BLF, Goh SMX, Chai YH, Loy ACM, Cheah KW, Yiin CL, Lock SSM. Thermo-catalytic co-pyrolysis of palm kernel shell and plastic waste mixtures using bifunctional HZSM-5/limestone catalyst: kinetic and thermodynamic insights. J. Energy Inst. 2023;107:101194.
[55] Kumar Mishra R, Mohanty K. Kinetic analysis and pyrolysis behavior of low-value waste lignocellulosic biomass for its bioenergy potential using thermogravimetric analyzer. Mater Sci Energy Technol 2021;4:136–47.
[56] Deng N, Zhang Y-f, Wang Y. Thermogravimetric analysis and kinetic study on pyrolysis of representative medical waste composition. Waste Manag 2008;28:1572–80.
[57] Suriapparao DV, Gautam R, Jeeru LRao. Analysis of pyrolysis index and reaction mechanism in microwave-assisted ex-situ catalytic co-pyrolysis of agro-residual and plastic wastes. Bioresour Technol 2022;357:127357.
[58] Jain AA, Mehra A, Ranade VV. Processing of TGA data: analysis of isoconversional and model fitting methods. Fuel 2016;165:490–8.
[59] Huang YW, Chen MQ, Li Y. An innovative evaluation method for kinetic parameters in distributed activation energy model and its application in thermochemical process of solid fuels. Thermochim Acta 2017;655:42–51.
[60] Dhaundiyal A, Singh SB. Fuzzification of distributed activation energy model using the Weibull distribution. J. nat. resour. dev. 2018;8:01–8.
[61] Xu D, Chai M, Dong Z, Rahman MM, Yu X, Cai J. Kinetic compensation effect in logistic distributed activation energy model for lignocellulosic biomass pyrolysis. Bioresour Technol 2018;265:139–45.
[62] Miura K, Maki T. A simple method for estimating f(E) and k0(E) in the distributed activation energy model. Energy Fuel 1998;12:864–9.
[63] Chantanumat Y, Phetwarotai W, Sangthong S, Palamanit A, Abu Bakar MS, Cheirsilp B, Phusunti N. Characterization of bio-oil and biochar from slow pyrolysis of oil palm plantation and palm oil mill wastes. Biomass Convers Biorefin 2022.
[64] Detchusananard T, Wuttipisan N, Limleamthong P, Prasertcharoensuk P, Maréchal F, Arpornwichanop A. Pyrolysis and gasification integrated process of empty fruit bunch for multi-biofuels production: technical and economic analyses. Energy Convers Manag 2022;258:115465.
[65] Handoko S, Nurhadi N, mujiati S, Fitriani R. Characterization of pyrolysis products of oil palm empty fruit bunch. IOP Conf Ser: Earth Environ Sci 2021;749:012041.
[66] Eke J, Onwudili JA, Bridgwater AV. Influence of moisture contents on the fast pyrolysis of trommel fines in a bubbling fluidized bed reactor. Waste Biomass Valorizat 2020;11:3711–22.
[67] Terry LM, Wee MXJ, Chew JJ, Khaerudini DS, Timuda GE, Aqsha A, Saptoro A, Sunarso J. Co-pyrolysis of oil palm trunk and polypropylene: pyrolysis oil composition and formation mechanism. S Afr J Chem Eng 2023;43:348–58.
[68] Chireshe F, Collard F-X, Görgens JF. Production of low oxygen bio-oil via catalytic pyrolysis of forest residues in a kilogram-scale rotary kiln reactor. J Clean Prod 2020;260:120987.
[69] Lin X, Zhang Z, Wang Q, Sun J. Interactions between biomass-derived components and polypropylene during wood–plastic composite pyrolysis. Biomass Convers Biorefin 2020.
[70] Ding Y, Huang B, Wu C, He Q, Lu K. Kinetic model and parameters study of lignocellulosic biomass oxidative pyrolysis. Energy 2019;181:11–7.
[71] Nawaz A, Kumar P. Thermal degradation of hazardous 3-layered COVID-19 face mask through pyrolysis: kinetic, thermodynamic, prediction modelling using ANN and volatile product characterization. J Taiwan Inst Chem Eng 2022;139:104538.

[72] Embaye TM, Ahmed MB, Deng N, Cui W, Bukhsh K, Zhang L, Zhu L, Wang X. Co-pyrolysis behavior of municipal solid waste and food waste residue: a thermogravimetric study to discern synergistic effect. Process Saf Environ Protect 2024;189:1274–84.
[73] Bhavanam A, Sastry RC. Kinetic study of solid waste pyrolysis using distributed activation energy model. Bioresour Technol 2015;178:126–31.
[74] Hou Y, Feng Z, He Y, Gao Q, Ni L, Su M, Ren H, Liu Z, Hu W. Co-pyrolysis characteristics and synergistic interaction of bamboo residues and disposable face mask. Renew Energy 2022;194:415–25.
[75] Supramono D, Sitorus AF, Nasikin M. Synergistic Effect on the Non-Oxygenated Fraction of Bio-Oil in Thermal Co-Pyrolysis of Biomass and Polypropylene at Low Heating Rate. Processes 2020;8:57.
[76] Karunakaran V, Abd-Talib N, Yong T-LKelly. Lignin from oil palm empty fruit bunches (EFB) under subcritical phenol conditions as a precursor for carbon fiber production. Mater Today: Proc 2020;31:100–5.
[77] Sidek FN, Saleh S, Abdul Samad NAF. Kinetic parameter estimation for pyrolysis of empty fruit bunch using model-fitting and model-free methods. Mater Today: Proc 2022;57:1241–7.
[78] Surahmanto F, Saptoadi H, Sulistyo H, Rohmat TA. Investigation of the slow pyrolysis kinetics of oil palm solid waste by the distributed activation energy model. Biofuels 2020;11:663–70.
[79] Yangali P, Celaya AM, Goldfarb JL. Co-pyrolysis reaction rates and activation energies of West Virginia coal and cherry pit blends. J Anal Appl Pyrolysis 2014;108:203–11.
[80] Montero-Calderón C, Tacuri R, Solís H, De-La-Rosa A, Gordillo G, Araujo-Granda P. Masks thermal degradation as an alternative of waste valorization on the COVID-19 pandemic: a kinetic study. Heliyon 2023;9:e13518.
[81] Mian I, Li X, Jian Y, Dacres OD, Zhong M, Liu J, Ma F, Rahman N. Kinetic study of biomass pellet pyrolysis by using distributed activation energy model and Coats Redfern methods and their comparison. Bioresour Technol 2019;294:122099.
[82] Mallick D, Poddar MK, Mahanta P, Moholkar VS. Discernment of synergism in pyrolysis of biomass blends using thermogravimetric analysis. Bioresour Technol 2018;261:294–305.